Estimation of SO_2 emissions using OMI retrievals

V. E. Fioletov,[1] C. A. McLinden,[1] N. Krotkov,[2] M. D. Moran,[1] and K. Yang[2,3]

Received 22 August 2011; revised 4 October 2011; accepted 10 October 2011; published 9 November 2011.

[1] Satellite sulfur dioxide (SO_2) measurements from the Ozone Monitoring Instrument (OMI) satellite sensor, averaged over a period of several years, were compared with emissions inventories for major US sources. Low- and high-spatial frequency filtration was applied to OMI data to reduce the noise and bias to enhance and reveal weak SO_2 signals that are otherwise not readily apparent. Averaging a large number of individual observations enables the study of SO_2 spatial distributions near larger SO_2 emissions sources with an effective resolution superior to that of an individual OMI observation and even to obtain rough estimates of the emissions level from those sources. It is demonstrated that individual sources (or multiple sources within 50 km) with annual SO_2 emissions greater than about 70 kT y^{-1} produce a statistically significant signal in 3-year averaged OMI data. A correlation of 0.93 was found between OMI SO_2 integrated around the source and the annual SO_2 emission rate for the sources greater than 70 kT y^{-1}. OMI SO_2 data also indicate a 40% decline in SO_2 values over the largest US coal power plants between 2005–2007 and 2008–2010, a value that is consistent with the reported 46% reduction in annual emissions due to the implementation of new SO_2 pollution control measures over this period. **Citation:** Fioletov, V. E., C. A. McLinden, N. Krotkov, M. D. Moran, and K. Yang (2011), Estimation of SO_2 emissions using OMI retrievals, *Geophys. Res. Lett.*, *38*, L21811, doi:10.1029/2011GL049402.

1. Introduction

[2] Satellite SO_2 observations have been used to monitor plumes from volcanic eruptions [e.g., *Krueger et al.*, 2000] and to calculate volcanic SO_2 budgets. More recently, it was demonstrated that satellite instruments can also detect SO_2 signals from anthropogenic sources [e.g., *Eisinger and Burrows*, 1998; *Carn et al.*, 2007; *Georgoulias et al.*, 2009; *Lee et al.*, 2011] and even study the evolution of emissions from very large source regions, e.g., in China [*Witte et al.*, 2009; *Li et al.*, 2010]. Recent retrieval algorithms applied to the Ozone Monitoring Instrument (OMI) on NASA's Aura spacecraft were specifically developed to retrieve total column SO_2 in the boundary layer [*Krotkov et al.*, 2006] and to monitor SO_2 from anthropogenic pollution sources.

[3] OMI provides the best horizontal resolution (13 × 24 km^2 footprint at nadir) among instruments in its class. However, even with this resolution, most anthropogenic sources produce elevated SO_2 levels that are detectable only within the co-located space of just one or two pixels. The same limitation applies to the standard archived OMI level 2G grid with resolution of 0.125° by 0.125°. This study employs a different analysis technique in which a large number of individual observations are used in an attempt to quantify the SO_2 spatial distributions near larger SO_2 emissions sources.

2. Data and Analysis

2.1. SO_2 Emissions Sources

[4] The top 100 largest US individual sources (according to the U.S. national emissions inventory for 2005: see http://www.epa.gov/ttn/chief/eiinformation.html) were examined in this study. The majority of these sites are coal-burning power plants. As will be demonstrated later, only ~40 of the largest sources, those with SO_2 emissions levels greater than ~60 kT y^{-1}, produce a statistically significant signal in the OMI data. The inventory data for these sources, unlike most emissions data, were based on direct stack measurements using Continuous Emissions Monitoring Systems as mandated by Title IV of the 1990 U.S. Clean Air Act Amendments (Public Law 101-549) (e.g., http://www.epa.gov/air/caa/title4.html). For the comparison with satellite data, it was assumed that emissions from these sources are constant throughout the year.

2.2. OMI SO_2 Data Product

[5] The Dutch-Finnish-built Ozone Monitoring Instrument (OMI) is a nadir-viewing, UV-visible spectrometer [*Levelt et al.*, 2006] that has been observing aerosols and trace gases, including SO_2, from the NASA EOS Aura satellite platform since 2004 [*Schoeberl et al.*, 2006]. This study focuses on anthropogenic pollution sources that emit SO_2 to the planetary boundary layer (PBL), and therefore a data product specifically designed to represent boundary-layer SO_2 was used [*Krotkov et al.*, 2006]. Values are given as total column SO_2 retrievals optimized for the PBL in Dobson Units (DU), where 1 DU is equal to $2.69 \cdot 10^{26}$ molec·km^{-2}. OMI SO_2 data for the period 2005–2010 were analyzed. The OMI measures 60 cross-track positions (pixels), and the pixel size varies depending on the track position from 13 × 24 km^2 at nadir to about 28 × 150 km^2 at the outermost swath angle. Data from the first and last 10 track positions were excluded from the analysis to limit the across-track pixel width to about 40 km. Beginning in 2007, some track positions were affected by field-of–view blockage and scattered light (so called, "row anomaly", see http://www.knmi.nl/omi/research/product/rowanomaly-background.php). The affected pixels were excluded from the analysis. Only clear sky data, defined as having a cloud radiance fraction (across each pixel) less than

[1]Environment Canada, Toronto, Ontario, Canada.
[2]Laboratory for Atmospheres, NASA Goddard Space Flight Center, Greenbelt, Maryland, USA.
[3]Department of Atmospheric and Oceanic Sciences, University of Maryland, College Park, Maryland, USA.

0094-8276/11/2011GL049402

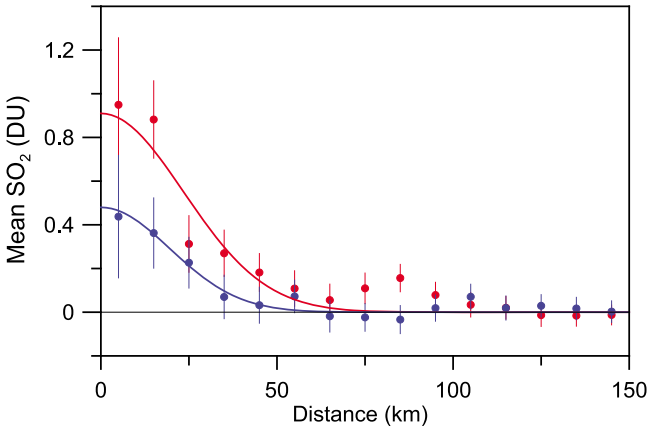

Figure 1. Mean OMI total column SO_2 for Bowen power station with annual emissions of about 170 kT y^{-1} (red) and Belews Creek power station (88 kT y^{-1}) (blue) as a function of the distance between the station and the pixel centre. The local bias was removed as discussed in the text. The error bars show the 95% confidence intervals for the mean. The best fits by Gaussian function are also shown. The secondary maximum on the Bowen curve is caused by the contribution of two power plants located about 80 km to the south.

20%, were used. To exclude cases of transient volcanic SO_2, the range of analyzed values were limited to a maximum of 5 DU. Furthermore, results presented in this study are based on May–August data only. While results for the rest of the year are similar, they exhibit larger uncertainties due to various factors such as larger solar zenith angles, variable surface albedo (snow), higher ozone optical depth, etc.

2.3. Spatial Smoothing and Local Bias Correction

[6] Figure 1 shows the mean column SO_2 values for the 2005–2007 period plotted as a function of a distance between the OMI pixel center and the location of two large emissions sources: the largest US SO_2 source (Bowen power plant in Georgia, estimated at 170 kT y^{-1}) and the 20th-largest source (Belews Creek power plant in North Carolina, 88 kT y^{-1}). As Figure 1 demonstrates, OMI data show elevated SO_2 values near the emissions sources but they became insignificant beyond about 50 km, even for the largest single source used in this study. This may explain why many sources are not typically seen by OMI: SO_2 from such sources affects only 1–2 pixels and the noise level is high. However, Figure 1 also suggests that it is possible to obtain a statistically significant signal by averaging a large number of individual pixels centered within a several km radius from the source. It was found that averaging over 3 years of data typically produces a statistically significant (at the 95% confidence level) mean value if the source annual emission is greater than ~70 kT y^{-1}, although some of the sources with the annual emissions of ~60 kT y^{-1} also produce significant mean values.

[7] Based on this finding, we use this pixel-averaging approach to analyze the long-term mean spatial SO_2 distribution near the source. For this, a geographical grid is established around the source and the average of all OMI pixels centered within a several km radius from each grid point is calculated. This approach is illustrated in Figure 2a. For Figure 2a, a 60 km × 60 km grid with a 2 km step was centered over the 10th-largest source, the John E. Amos power plant in West Virginia. An average of all SO_2 data falling within a 12 km radius of the center of a grid cell was assigned to that grid point, where the pixel center is used as the location of the measurement. The resultant distribution of SO_2 values, presented in Figure 2a, reveals the highest mean SO_2 values occurred at grid points located within a small area around the source. Thus, this procedure provides a detailed "subpixel-resolution" spatial distribution of long-term mean SO_2 value in the vicinity of the source. The choice of averaging radius determines the degree of smoothing:

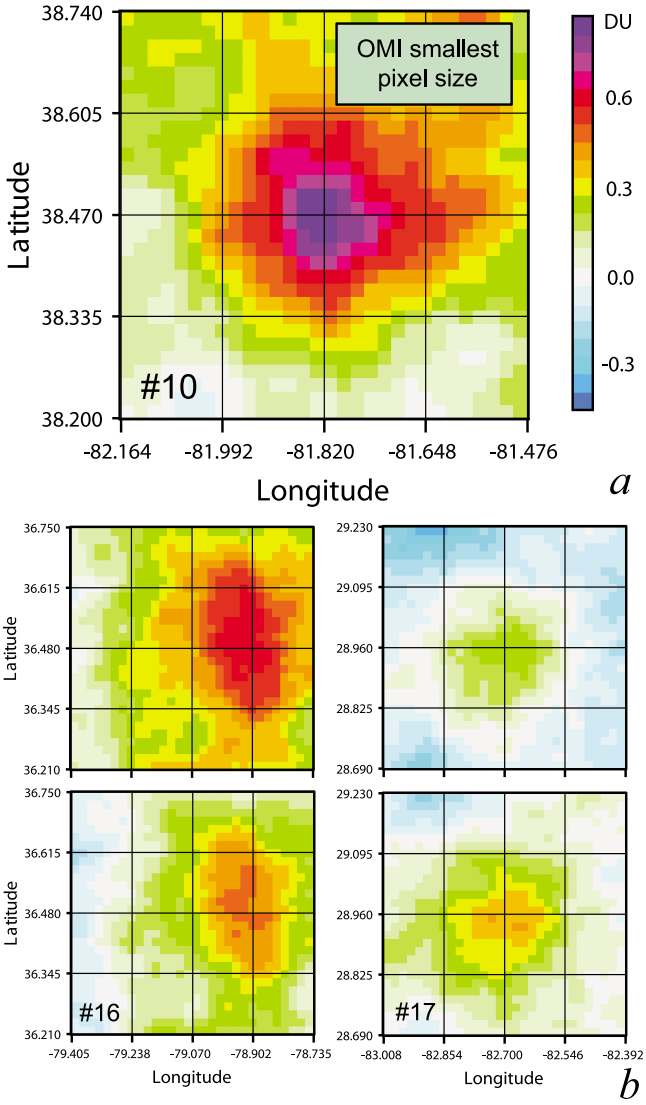

Figure 2. (a) Mean summertime OMI total-column SO_2 around the 10th-largest US SO_2 source (102 kT y^{-1}), the John E. Amos power plant, located in the center. For this plot, a 2 × 2 km grid around the plant was set up and for each grid point, all overpasses centered within 12 km from that point were averaged. The smallest OMI pixel is shown for reference. (b) Similar plots for the 16th-largest source (Roxboro power plant, North Carolina) and 17th-largest source (Crystal River power plant, Florida) (bottom) with and (top) without local bias removed (see text). Both sources emitted nearly the same amount of SO_2 (about 93 kT y^{-1}).

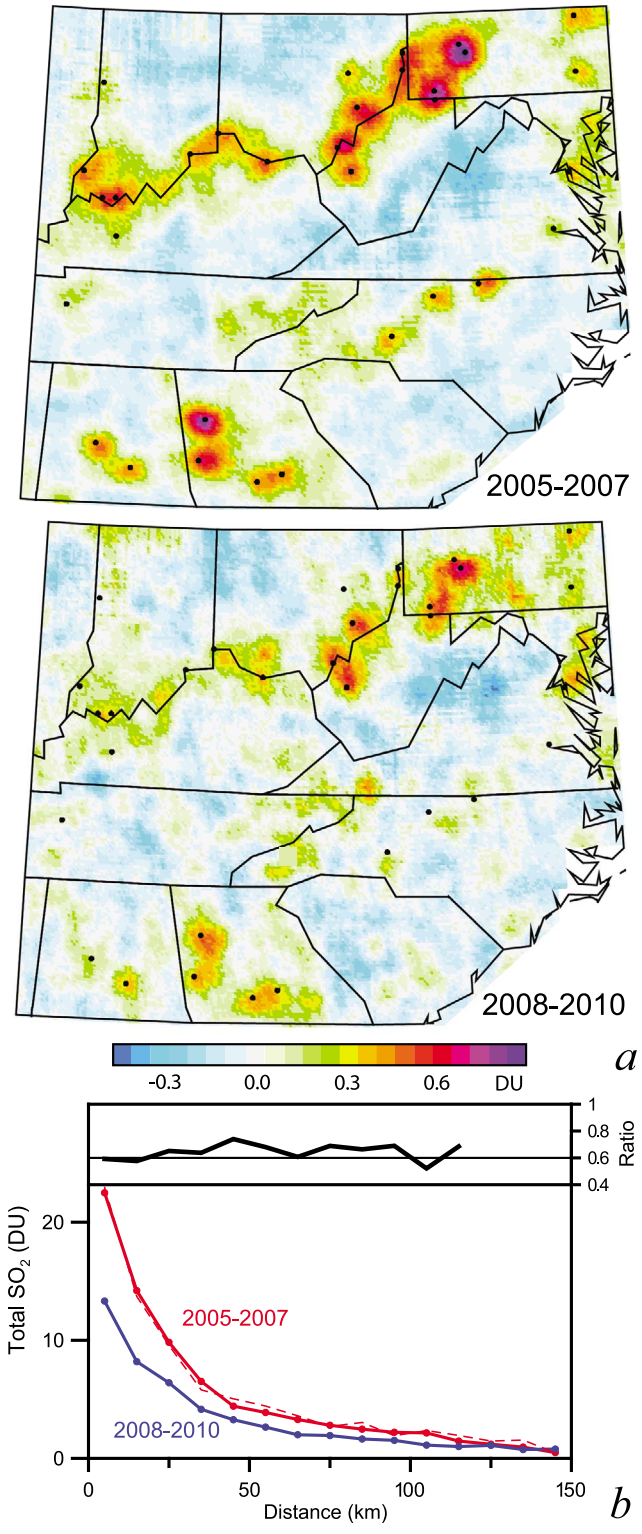

Figure 3. (a) Mean OMI SO_2 values over the Eastern US for 2005–2007 and 2008–2010. The dots indicate emission sources from the top 40 sources list. (b) The sum of SO_2 values from the top 40 emission sources as a function of distance from the source for 2005–2007 (red) and 2008–2010 (blue). The ratio between the 2008–2010 and 2005–2007 values is shown at the top of Figure 3b. The dashed red line represents the results for 2005–2007 when only track positions from 11 to 24 were used (i.e., those that were operational in 2010).

averaging with a large radius reduces the noise, but it also reduces the spatial resolution.

[8] Systematic errors in retrieved SO_2 resulting from imperfect instrument calibration as well as from, for example, forward model simplifications, were substantially reduced in the present OMI algorithm by empirical corrections [*Yang et al.*, 2007]. Nonetheless, some large-scale biases remain. It can be expected that, other factors being the same (e.g., average solar illumination angles, wind speed, cloud cover, surface albedo), sources with similar emission strengths should produce similar mean observed SO_2 values. As Figure 2b shows, this is not always the case and residual biases are comparable with the mean SO_2 values from the sources. Since these biases appear as large-scale patterns, they can be removed with a spatial high-pass filter. To accomplish this, SO_2 values within a 300 km radius were averaged and then this mean value was subtracted. It was also found that these local biases are somewhat different from year to year so that the local bias correction was calculated for each year. Mean SO_2 values around similar sources corrected in this manner are very similar as illustrated by Figure 2b.

[9] This combination of spatial smoothing and local bias correction can be used to produce high-resolution, long-term mean SO_2 maps. Figure 3a presents such maps for the eastern US, where the majority of large SO_2 sources are located (indicated by the black dots). Areas of high SO_2 values are centered over these major emissions sources. The maps in Figure 3 were generated for two 3-year intervals, 2005–2007 and 2008–2010. A 24 km averaging-radius was used to smooth the data for this plot. A substantial decline in OMI SO_2 values at major sources between the two time intervals is evident from Figure 3. This reduction is attributed to the installation of additional flue-gas desulfurization units (or "scrubbers") at many US power plants over this period (e.g., http://www.epa.gov/airmarkets/images/CoalControls.pdf) to meet stricter emissions limits introduced by the Clean Air Interstate Rule.

[10] OMI data can be further used to evaluate the reduction in the measured SO_2 values and then compared to the actual reported reduction in emissions levels. The sum of SO_2 values from the top 40 US emissions sources was calculated (this corresponds to sources with annual emissions greater than 60 kT y^{-1}) as a function of distance from the source for 2005–2007 and 2008–2010 and is shown in Figure 3b. For this plot, the mean SO_2 value was calculated for each source as a function of distance from the source and then these mean values were added up to form the sum. The ratio between the two sums is about 0.6, indicating a 40% reduction in OMI mean SO_2 values. The actual measured reduction for these same sources over this period based on emission reported to the U.S. Environmental Protection Agency (see http://camddataandmaps.epa.gov/gdm/index.cfm?fuseaction=emissions.wizard) was 46%.

3. Emissions Inventories and OMI SO_2 Values

[11] Assuming comparable SO_2 sources produce similar long-term mean OMI SO_2 values, OMI SO_2 can be related to emissions levels from individual sources and furthermore, provide an estimate of annual emissions. In order to quantify the total amount of SO_2 near a source, a two-dimensional

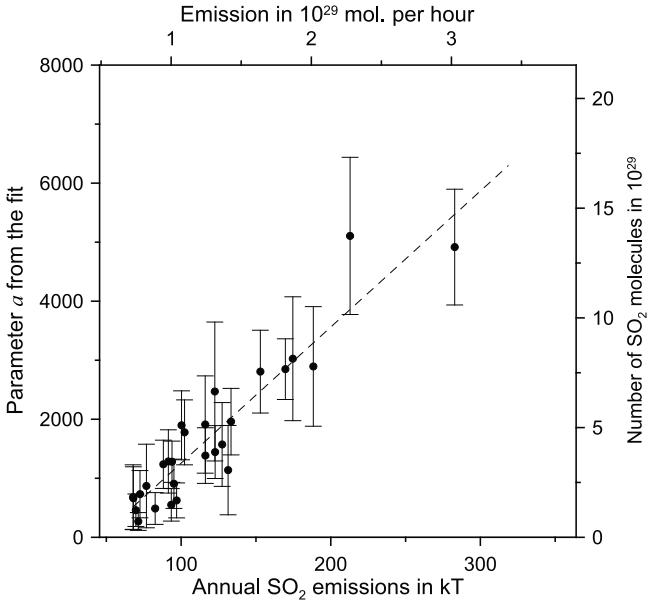

Figure 4. A scatter plot of annual SO_2 emission from the largest US sources in 2005 vs. mean OMI SO_2 for 2005–2007 integrated around the source estimated using the best fits by 2D Gaussian function (1). Emissions are given in kT y^{-1} and molec h^{-1} units calculated assuming a constant emission rate. The integrated OMI values are presented as the parameter a (in $2.69 \cdot 10^{26}$ molec) from the fit in number of molecules. If two or three sources are located in a close proximity, they were counted as a single source with the total emission equal to the sum of emissions from these sources. The error bars represent the 95% confidence intervals.

Gaussian function $OMI_{SO_2} = a \cdot f(x, y)$ was fit to OMI SO_2 measurements within a time window and radius, where

$$f(x,y) = \frac{1}{2\pi\sigma_x\sigma_y\sqrt{1-\rho^2}}\exp\left(-\frac{1}{2(1-\rho^2)}\left[\frac{(x-\mu_x)^2}{\sigma_x^2}+\frac{(y-\mu_y)^2}{\sigma_y^2}-\frac{2\rho(x-\mu_x)(y-\mu_y)}{\sigma_x\sigma_y}\right]\right) \quad (1)$$

and x and y refer to the co-ordinates of the OMI pixel center. Note that actual OMI measurements, not smoothed data described in section 2 were used for the fit. The elliptical shape of the SO_2 distribution near the source is determined by parameters σ_x, σ_y, and ρ. The parameters μ_x and μ_y were included since the position of the emissions source may be different from the position of the fit maximum due to for example, prevailing winds or if the source is comprised of two closely located power plants. Since $\int_{-\infty}^{\infty}\int_{-\infty}^{\infty} f(x,y)dxdy = 1$, the parameter a represents the total observed number of SO_2 molecules near the source. If OMI_{SO_2} is in DU, i.e., in $2.69 \cdot 10^{26}$ molec km^{-2}, and σ_x, σ_y are in km, then a is in $2.69 \cdot 10^{26}$ molec. For SO_2 emissions sources less than 140 kT y^{-1}, the fitting was done using OMI pixels centered within a 40 km radius from a source and local bias was removed. For sources larger than 140 kT y^{-1} that affect SO_2 values at greater distances, the radius was 60 km. Note that function (1) has a single maximum and therefore describes an SO_2 distribution near a single source. If two or three sources are located in a close proximity (within 50 km for very large sources), they were counted as a single source with the total emissions equal to the sum of emissions from these sources. Otherwise, instances where the secondary source was located within the fitting radius were excluded from the analysis.

[12] The scatter plot of the total number of SO_2 molecules retrieved from the OMI measurements, a, versus daily SO_2 emissions strength for each source location is shown in Figure 4. The 2005–2007 period was used in Figure 4 because the emissions were fairly stable during that period. Sources emitting less that 70 kT y^{-1} typically produced values of a that were not statistically significant and were not shown in the plot. Thus 70 kT y^{-1} represents the threshold for which this methodology can be applied to the present OMI SO_2 data. The correlation coefficient between total molecules and annual emission is 0.93 and this high degree of correlation implies that SO_2 emissions can be estimated from OMI data using a linear regression.

[13] There is also a physical interpretation of this relationship since the slope of the regression line represents the effective SO_2 removal time due to advection, deposition and chemical conversion to sulfate aerosols. Its value, 5 hours, is 3–5 times less than the current estimates for the eastern US in summer [*Lee et al.*, 2011]. Possible reasons for this discrepancy include the use of a constant air mass factor (AMF) in deriving vertical columns, neglecting dry deposition, dispersion due to variable wind speeds, and statistical arguments. Moreover, it is unclear if a lifetime, obtained from a model simulation at ~200 km resolution, is representative within several km of the emission site. A constant AMF is reasonable given that the majority of locations considered were in the eastern US and so to first order, any error in AMF will be common to most locations [*Lee et al.*, 2009]. Clearly, detailed AMFs based on local conditions, including a realistic representation of aerosols (which are likely elevated near large pollution sources), are necessary to establish a quantitative link or to expand the analysis to other regions. Another contributing factor is that satellite retrievals may consistently underestimate the small (compared to the pixel sizes) emission plumes, because they do not usually occupy the entire pixel footprint [*Yang et al.*, 2010]. Furthermore on average advection and deposition may be the prevailing removal mechanisms in the vicinity of the power plants. The power plants in the eastern US are located in an area of typically weak summer winds, days with stronger winds causing a faster dispersion of the SO_2 plume still contribute to the overall statistics.

4. Summary and Discussion

[14] Pollution plumes from individual power plants are not typically detectable in daily OMI SO_2 maps using standard analysis techniques. However it is possible to obtain a statistically significant signal from large sources (>70 kT y^{-1}) by averaging OMI SO_2 pixels centered in 10–20 km from the source over a period of several years. For such large sources, there is a high correlation (0.93) between the annual emissions from an individual source and mean summertime SO_2 integrated over the area around that source.

[15] A pixel-averaging technique, i.e., averaging a large number of individual OMI pixels, together with a local bias correction (i.e., low- and high- spatial frequency filtration)

were used to map the mean distribution around the major sources and to produce a composite SO_2 maps for the eastern US. Such maps for 2005–2007 and 2008–2010 periods demonstrate a substantial decline in SO_2. Moreover, the mean OMI SO_2 values summed near 40 largest emissions sources were 40% lower in 2008–2010 than in 2005–2007, consistent with the measured 46% reduction in emissions due to the implementation of new SO_2 pollution control measures at some sources over this period.

[16] Large errors of individual OMI SO_2 retrievals and large pixel size (~300 km^2) are the main reasons why sources with emissions below 70 kT y^{-1} typically do not produce a statistically significant signal in OMI observations. Smaller sources may be detectable in the future if the algorithm is improved. Ultimately, the proposed technique will work best with frequent high spatial resolution measurements from the future GEO-CAPE UV imaging spectrometer on geostationary satellite [*Fishman et al.*, 2008]. The unprecedented temporal and spatial resolution possible from geostationary vintage point will offer the best possibilities for monitoring emissions and understanding pollution processes.

[17] **Acknowledgments.** We acknowledge the NASA Earth Science Division for funding of OMI SO_2 product development and analysis. The Dutch-Finnish-built OMI instrument is part of the NASA EOS Aura satellite payload. The OMI project is managed by KNMI and the Netherlands Agency for Aero-space Programs (NIVR). The US Environmental Protection Agency provided SO_2 emissions data. The authors also thank two anonymous reviewers for their thorough and thoughtful comments.

[18] The Editor thanks two anonymous reviewers for their assistance in evaluating this paper.

References

Carn, S. A., A. J. Krueger, N. A. Krotkov, K. Yang, and P. F. Levelt (2007), Sulfur dioxide emissions from Peruvian copper smelters detected by the Ozone Monitoring Instrument, *Geophys. Res. Lett.*, *34*, L09801, doi:10.1029/2006GL029020.

Eisinger, M., and J. P. Burrows (1998), Tropospheric sulfur dioxide observed by the ERS-2 GOME instrument, *Geophys. Res. Lett.*, *25*, 4177–4180, doi:10.1029/1998GL900128.

Fishman, J., et al. (2008), Remote sensing of tropospheric pollution from space, *Bull. Am. Meteorol. Soc.*, *89*(6), 805–821, doi:10.1175/2008BAMS2526.1.

Georgoulias, A. K., D. Balis, M. E. Koukouli, C. Meleti, A. Bais, and C. Zerefos (2009), A study of the total atmospheric sulfur dioxide load using ground-based measurements and the satellite derived Sulfur Dioxide Index, *Atmos. Environ.*, *43*, 1693–1701, doi:10.1016/j.atmosenv.2008.12.012.

Krotkov, N. A., S. A. Carn, A. J. Krueger, P. K. Bhartia, and K. Yang (2006), Band residual difference algorithm for retrieval of SO_2 from the Aura Ozone Monitoring Instrument (OMI), *IEEE Trans. Geosci. Remote Sens.*, *44*, 1259–1266, doi:10.1109/TGRS.2005.861932.

Krueger, A. J., S. J. Schaefer, N. Krotkov, G. Bluth, and S. Barker (2000), Ultraviolet remote sensing of volcanic emissions, in *Remote Sensing of Active Volcanism*, *Geophys. Monogr. Ser.*, vol. 116, edited by P. J. Mouginis-Mark, J. A. Crisp, and J. H. Fink, pp. 25–43, AGU, Washington, D. C., doi:10.1029/GM116p0025.

Lee, C., R. V. Martin, A. van Donkelaar, G. O'Byrne, N. Krotkov, A. Richter, L. G. Huey, and J. S. Holloway (2009), Retrieval of vertical columns of sulfur dioxide from SCIAMACHY and OMI: Air mass factor algorithm development, validation, and error analysis, *J. Geophys. Res.*, *114*, D22303, doi:10.1029/2009JD012123.

Lee, C., et al. (2011), SO_2 emissions and lifetimes: Estimates from inverse modeling using in situ and global, space-based (SCIAMACHY and OMI) observations, *J. Geophys. Res.*, *116*, D06304, doi:10.1029/2010JD014758.

Levelt, P. F., G. H. J. van den Oord, M. R. Dobber, A. Mälkki, H. Visser, J. de Vries, P. Stammes, J. Lundell, and H. Saari (2006), The Ozone Monitoring Instrument, *IEEE Trans. Geosci. Remote Sens.*, *44*(5), 1093–1101, doi:10.1109/TGRS.2006.872333.

Li, C., Q. Zhang, N. A. Krotkov, D. G. Streets, K. He, S.-C. Tsay, and J. F. Gleason (2010), Recent large reduction in sulfur dioxide emissions from Chinese power plants observed by the Ozone Monitoring Instrument, *Geophys. Res. Lett.*, *37*, L08807, doi:10.1029/2010GL042594.

Schoeberl, M. R., et al. (2006), Overview of the EOS Aura mission, *IEEE Trans. Geosci. Remote Sens.*, *44*(5), 1066–1074, doi:10.1109/TGRS.2005.861950.

Witte, J. C., M. R. Schoeberl, A. R. Douglass, J. F. Gleason, N. A. Krotkov, J. C. Gille, K. E. Pickering, and N. Livesey (2009), Satellite observations of changes in air quality during the 2008 Beijing Olympics and Paralympics, *Geophys. Res. Lett.*, *36*, L17803, doi:10.1029/2009GL039236.

Yang, K., N. A. Krotkov, A. J. Krueger, S. A. Carn, P. K. Bhartia, and P. F. Levelt (2007), Retrieval of large volcanic SO_2 columns from the Aura Ozone Monitoring Instrument: Comparison and limitations, *J. Geophys. Res.*, *112*, D24S43, doi:10.1029/2007JD008825.

Yang, K., X. Liu, P. K. Bhartia, N. A. Krotkov, S. A. Carn, E. J. Hughes, A. J. Krueger, R. J. D. Spurr, and S. G. Trahan (2010), Direct retrieval of sulfur dioxide amount and altitude from spaceborne hyperspectral UV measurements: Theory and application, *J. Geophys. Res.*, *115*, D00L09, doi:10.1029/2010JD013982.

V. E. Fioletov, C. A. McLinden, and M. D. Moran, Environment Canada, Toronto, ON M3H 5T4, Canada. (vitali.fioletov@ec.gc.ca)

N. Krotkov and K. Yang, Laboratory for Atmospheres, NASA Goddard Space Flight Center, Greenbelt, MD 20771, USA.